Disorder and Structure in the Rab11 Binding Domain of Rab11 Family Interacting Protein 2[†,‡]

Jie Wei, Yuqi Liu, Kakoli Bose,[§] Gillian D. Henry, and James D. Baleja*

Department of Biochemistry, Tufts University School of Medicine, Boston, Massachusetts 02111

Received October 29, 2008; Revised Manuscript Received December 8, 2008

ABSTRACT: Rab11 plays a central role in plasma membrane recycling which returns cellular receptors for reuse at the cell surface. A recently identified family of Rab11 interacting proteins (FIP) includes FIP2. The C-terminal region of FIP2 is essential for colocalization with Rab11 on early endosomes and for enabling formation of higher-order oligomers. Rab11 binding and oligomerization of FIP2 are separable. Here we have determined the three-dimensional structure of the 40-residue coiled-coil oligomerization domain of FIP2 in the absence of Rab11 using NMR methods. The N-terminal half showed strong NOE cross-peaks and well-dispersed NMR resonances, whereas the C-terminal half had fewer NOE cross-peaks and less chemical shift dispersion. The 10 C-terminal residues were mostly disordered. The final structures of the dimer had favorable Ramachandran angles and a root-mean-square deviation of 0.59 ± 0.13 Å over superimposed backbone residues. The structure allows a comparison to a structure of FIP2 in complex with Rab11 that was determined crystallographically. In complex with Rab11, the C-terminal residues are not disordered but have a helical structure that predicts residual dipolar coupling constants that are incompatible with those measured on the unbound FIP2. In both structures, a histidine residue is found at the normally hydrophobic position of the heptad repeat of the coiled coil, and here we show its ionization destabilizes the coiled-coil structure. Together, these data allow us to build a model in which the binding of FIP family proteins to Rab11 can be described in terms of conformational changes and that suggests new modes of regulation.

Eukaryotic cells internalize nutrients, fluids, and other molecules from the extracellular environment through the plasma membrane via a process called endocytosis. The Rab protein family members regulate vesicle tethering and docking with target membranes and ensure the precision of vesicle fusion. In particular, Rab11 plays a central role in plasma membrane recycling which returns cellular receptors for reuse at the surface (*1, 2*).

Rab11 conducts its biological effects by interacting with effector proteins in a GTP-dependent manner. Rab11 behaves as a typical GTPase protein in which the GTP-bound form is active and the GDP-bound form is inactive. These two forms have different conformations in their switch 1 and switch 2 regions that are built on a scaffold of a central six-stranded β-sheet flanked by two α-helices on each side (*3*). The interacting region of the effector is generally a dimer of α-helices arranged in a coiled coil (*4*−*6*), although sometimes a helix is used to form a binding surface, but with structures different from a coiled coil (*7*−*9*).

A recently identified family of Rab11 interacting proteins (FIP) includes six members to date: Rab11-FIP1 (FIP1) (*10*), Rab11-FIP2 (FIP2)[1] (*10*), Rab11-FIP3 (FIP3/eferin) (*10*), Rab11-FIP4 (FIP4) (*11*), Rip11/FIP5 (*12*), and Rab coupling protein (RCP) (*13*). The FIP proteins share a highly homologous Rab11 binding domain at their C-termini, which overlaps a conserved region that mediates formation of a coiled coil (Figure 1). FIP2 is perhaps the most extensively studied of the FIP proteins and has distinct biological roles. FIP2 is unique in that it contains multiple (three) Asn-Pro-Phe (NPF) sequences that bind the EH domain of Reps1, thereby coordinating EGF receptor signaling (*14*). Rab11-FIP2 also coordinates functions of Rab11 with myosin Vb (*15*). The C-terminal region of FIP2 was found to be essential for its colocalization with Rab11 on early endosomes and enables FIP2 to form higher-order oligomers (*14*). For recycling of the transferrin receptor, expression of the C-terminal region of FIP2 induced aberrant tubulation of the compartment-containing transferrin receptors, which could not be reversed by overexpression of Rab11, thus underlining the importance of the C-terminal region of FIP2 in receptor recycling (*16*).

Our previous study of FIP2 defined the boundaries of the Rab11-FIP homology domain (RH domain) and found a 50-

[†] Supported in part by NIH Grant GM067985.

[‡] Atomic coordinates have been deposited with the Research Collaboratory for Structural Bioinformatics Protein Data Bank (entry 2K6S), and NMR assignments have been deposited in the BioMagResBank (BMRB) NMR structural database (accession number 15880).

* To whom correspondence should be addressed: Department of Biochemistry, 136 Harrison Ave., Tufts University School of Medicine, Boston, MA 02111. Phone: (617) 636-6872. Fax: (617) 636-2409. E-mail: jim.baleja@tufts.edu.

[§] Current address: ACTREC, KS-138, Plot 1 & 2, Sector 22, Kharghar, Navi Mumbai 410210, India.

[1] Abbreviations: CD, circular dichroism; FIP2, Rab11 functional interacting protein 2; HSQC, heteronuclear single-quantum coherence; NOE, nuclear Overhauser effect; RBD, Rab11 binding domain; RHCC, coiled-coil region of the Rab11-FIP homology domain; rms, root-mean-square.

10.1021/bi8020197 CCC: $40.75
Published on Web 01/02/2009

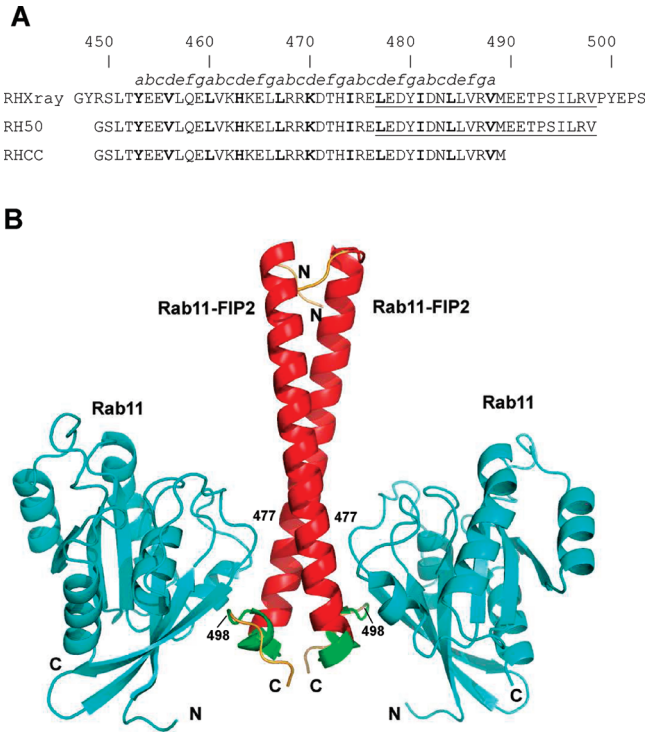

FIGURE 1: (A) Peptide sequences of Rab11-FIP2 containing the Rab11-FIP homology domain. The X-ray structure of Rab11-FIP2 bound to Rab11 (*9*) showed electron density for residues 447−503 (RHXray). The italic letters above the sequences denote the predicted heptad repeats within the coiled-coil domain. Residues in the *a* and *d* positions are in bold and participate in the formation of a hydrophobic interface. The region of Rab11-FIP2 (residues 477−498) that interacts with Rab11 (RBD) is underlined. The 50-residue RH50 domain contains the minimal regions needed for both Rab11 binding and formation of the coiled coil, whereas the shorter RHCC domain contains the minimal region needed for formation of the coiled coil (*17*). (B) Model of Rab11 in complex with Rab11-FIP2. The coordinates were from PDB entry 2GZH (*9*). The Rab11 molecules are colored cyan. The RHCC portion of Rab11-FIP2 is colored red, and the portion unique to RH50 is colored green. The boundaries (residues 477 and 498) of the Rab11 binding domain are indicated by residue numbers. Poorly structured residues at the N- and C-termini are colored orange.

residue segment (RH50) that formed a coiled coil and was able to bind Rab11 efficiently (Figure 1A). We showed that a preformed helical conformation was not necessary as constructs that exhibited little coiled-coil formation still interacted with Rab11 efficiently, and conversely a construct, RHCC, which had as much helical structure as RH50, did not bind Rab11. Limited proteolysis of RH50 showed that the 10 C-terminal residues were susceptible to cleavage and probably relatively disordered. These data are consistent with mutagenesis data on FIP2 that suggest Rab11 binding and oligomerization are separable, thus potentially representing distinct mechanisms of regulation in a cellular context (*14*).

The crystal structure of FIP2 in complex with Rab11 was determined while this work on FIP2 in the absence of Rab11 was in progress (*9*). Although the crystal was formed with a longer construct containing the last 100 residues of FIP2, the residues showing electron density (S450−V498) were nearly the same as in the proteolytically derived RH50 fragment (Figure 1). The overall crystal structure is a heterotetramer with dyad symmetry arranged as a Rab11−$(FIP2)_2$−Rab11 complex. Switch 1 of Rab11 is bound in a pocket between the two helices, while switch 2 remains flexible and is only peripherally associated with the effector. FIP2 forms an α-helical coiled coil which has a Rab11 binding patch on equivalent and opposite sides close to the C-terminus. The 10 C-terminal residues of FIP2 were distinctly not disordered but have a structure that is presumably induced by interaction with Rab11 and comprises an extension of the coiled coil by three residues, a turn, a 3_{10}-helix, a short *β*-strand, and a loop (*9*). At the interface, hydrogen bonds are observed between backbone atoms L496 and V498 of FIP2 and F48 of Rab11 as well as between R497 of FIP2 and T50 of Rab11 (*9*). We do not know the extent to which the structure in the absence of Rab11 resembles that in complex with Rab11, and therefore, we assessed the structures of RH50 and RHCC using NMR methods. More importantly, a dynamic perspective of the interaction is described in which the disorder in the unbound FIP2 protein permeates from the C-terminus into the coiled coil. Furthermore, a histidine residue is found at the hydrophobic "*d*" position of the heptad repeat, and we show that ionization of this histidine changes the FIP2 coiled-coil structure.

MATERIALS AND METHODS

Sample Preparation. The expression and purification of unlabeled RHCC and RH50 have been described in detail previously (*17*). Uniformly ^{15}N-labeled or ^{13}C-labeled domains were obtained by using M9 medium containing either 1 g/L [^{15}N]ammonium chloride or 2 g/L [^{13}C]glucose, respectively. To prepare samples selectively labeled with ^{15}N at particular amino acids, an M9 medium was used that lacked ammonium chloride and instead contained a mixture of unlabeled amino acids except for the appropriate ^{15}N-labeled amino acid (150 mg/L for leucine and 67 mg/L for lysine) (*18*). A construct with a mutation (H463A) was prepared by PCR methods and purified using the same procedure that was used for the wild type.

NMR Spectroscopy. Samples consisted of 0.8−1.2 mM domain in 20 mM phosphate (pH 7.3). Unless otherwise stated, all experiments were performed at 298 K on a Bruker Avance-600 spectrometer. Resonance assignments and NOE analyses were performed on a ^{15}N- and ^{13}C-labeled RHCC sample using a suite of gradient-enhanced NMR experiments as described previously (*19*). The backbone was assigned using mostly HNCA (*20*), HNCO (*20*), HN(CA)CO (*21*), HN(CO)CA (*22*), CBCANH (*22*), and CBCA(CO)NH (*20*) data, whereas the side chains were assigned using three-dimensional (3D) HCCH-TOCSY. NOEs were detected in a 3D NOESY-HSQC spectrum (^{15}N-separated) on a Bruker DMX 800 spectrometer for greater sensitivity at the higher field. $^{1}H-^{15}N$ residual dipolar couplings were measured using 10−15 mg/mL filamentous bacteriophage Pf1 as the alignment medium (*23*). To obtain unambiguous intermolecular NOEs, a two-dimensional (2D) ^{13}C-filtered, ^{13}C-selected NOESY spectrum was recorded on a sample comprising a mixture of 50% ^{12}C-labeled protein and 50% ^{13}C-labeled protein that was refolded from 4 M urea (*24*). 2D spectra were also recorded for RHCC in a 100% D_2O solution. ^{15}N T_2 and NOE experiments were performed at 15 °C on a Bruker Avance 600 MHz spectrometer (*25, 26*). All data were processed with Bruker XWINNMR. SPARKY was

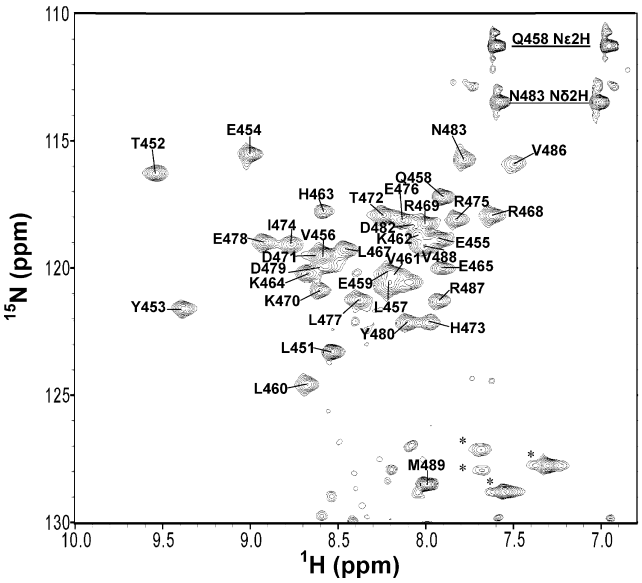

FIGURE 2: 2D ^{1}H−^{15}N HSQC spectrum of uniformly ^{15}N-labeled RHCC in 20 mM sodium phosphate buffer (pH 7.3) showing amide proton to nitrogen correlations that are labeled by residue number. Cross-peaks for the side chain amides of asparagine and glutamine are joined by horizontal lines labeled with their assignments. Peaks labeled with asterisks correspond to the Nε*H* protons of the four arginine side chains. Unlabeled peaks are impurities due to a small amount of degradation. The spectrum was collected at 600 MHz and 15 °C.

used for resonance assignment and measurement of NOE cross-peak intensities (*27*).

Conformational Data and Structure Calculations. NOEs used in structure calculation were measured from a 2D NOESY spectrum recorded in D_2O and from a 3D ^{1}H−^{15}N NOESY HSQC spectrum recorded in H_2O using a mixing time of 100 ms. Backbone dihedral angle restraints were derived from the secondary structure of the protein and the backbone chemical shift analysis program TALOS (*28*). Structures were calculated using CNS (version 1.1) (*29*) as described previously (*30*). The same calculation procedure was used for monomer and dimer structures, except for the fact that the latter used noncrystallographic dimer symmetry restraints for residues Y453−L485. The NOE/hydrogen bond and dihedral constraints used the default force constants (75 kcal/Å^2 and 400 kcal/deg^2, respectively). The *E*repel function was replaced with a Lennard-Jones potential during the final Powell minimization (*30*). Ten initial structures of the complex were calculated without the residual dipolar coupling restraints. Alignment tensor parameters (D_a and R) were determined using PALES (*31*). The residual dipolar coupling restraints were incorporated into the final calculation with a force scale from 0.01 to 50 kcal/Hz^2 in Cartesian space. The resulting 30 structures were validated by PROCHECK (*32*). Structural statistics were collected with PROCHECK. Structures were drawn using Pymol (DeLano Scientific, Palo Alto, CA) and MOLMOL 2k.2 (*33*).

Circular Dichroism. Far-UV CD spectra were recorded on a JASCO model 810 spectropolarimeter by averaging two scans with a step size of 0.5 nm using a cuvette with a path length of 0.1 cm. Spectra were baseline corrected by buffer subtraction. Peptide concentrations were determined by UV absorbance at 280 nm. The ellipticity at 222 nm was measured as a function of temperature for thermal denaturation studies.

Equilibrium Unfolding Studies. Protein samples (5 μM) and urea stock solutions (10 M) were prepared in acetate-phosphate buffer that was prepared by mixing 20 mM acetic acid, 200 mM NaCl, and 1 mM DTT with 20 mM Na_2HPO_4, 200 mM NaCl, and 1 mM DTT to the desired pH as described previously (*34*). Fluorescence emission scans were acquired between 290 and 350 nm using excitation at 280 nm using a Jobin-Yvon Fluorolog-3 fluorometer. The average emission wavelength ($\langle\lambda\rangle$) was determined for each fluorescence spectrum using eq 1:

$$\langle\lambda\rangle = \sum_{i=1}^{N} (I_i\lambda_i) / \sum_{i=1}^{N} (I_i) \quad (1)$$

where $\langle\lambda\rangle$ is the average emission wavelength and I_i is the emission at wavelength λ_i (*35*). Data were fit to a two-state dimer to monomer model as described by eq 2:

$$N_2 \overset{K_{eq}}{\longleftrightarrow} 2U \quad (2)$$

where the protein is assumed to be either in a native homodimeric state (N_2) or in an unfolded monomeric state (U) as described previously (*34*). Data were also fit to a two-state monomer to monomer model as described by eq 3:

$$N \overset{K_{eq}}{\longleftrightarrow} U \quad (3)$$

where the protein is assumed to be either in a native monomeric state (N) or in an unfolded monomeric state (U) as described previously (*36*). Δ*G* values were calculated as described previously (*34*).

RESULTS

Determination of the Three-Dimensional Structure of the RH Domain. Various constructs representing regions at the C-terminal end of Rab11-FIP2 were previously assessed by limited proteolysis in the absence of Rab11 (*17*). The circular dichroism spectra of RHCC and RH50 were also found to be nearly identical, suggesting that they have the same helical structure except for the additional C-terminal residues of RH50 which are disordered (*17*). The similarity in structure is consistent with ^{15}N−^{1}H correlation NMR spectra that show very similar resonance positions for the structured parts of the peptides (*37*). Because RHCC comprising residues 450−489 gave better quality NMR spectra, it was then used for further optimization and detailed structural analysis.

Increasing the temperature from 25 to 37 °C gave spectra with slightly narrower line widths, but fewer observable resonances in the ^{1}H−^{15}N HSQC spectrum. To reduce the level of hydrogen exchange, we lowered the pH from 7.4 to 6.8, but the protein precipitated. Altering the salt concentration and adding trifluoroethanol (TFE) did not produce significant improvement of the quality of the spectra. The best NMR spectra were recorded in 20 mM phosphate (pH 7.3) (Figure 2). Despite the optimization of the sample, resonance lines were broad with T_2 values of ∼35 ms (Figure 1S of the Supporting Information), while the T_2 value in a similarly sized coiled coil is ∼75 ms (*38*). The shorter T_2 indicates either aggregation or the presence of internal motion. Although the quality of NMR spectra did not substantially change using concentrations between 0.3 and

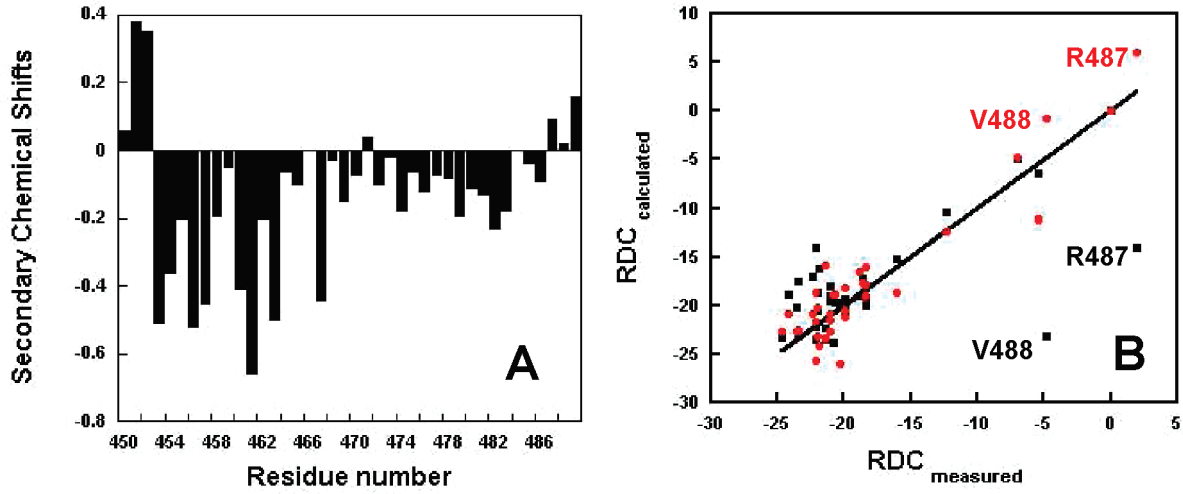

FIGURE 3: Structural assessment from chemical shifts and RDC data. (A) The Hα chemical shifts of residues in RHCC were compared with the Hα chemical shifts corresponding to a random coil conformation (secondary chemical shifts). (B) The fit of the experimental RDC data to that calculated from the X-ray model of RHCC (black squares) and NMR structure of RHCC (red circles). Two residues that fit the X-ray model poorly are labeled by residue number.

1.2 mM, a small degree of hexamer formation was noted in analytical ultracentrifugation experiments (*17*), suggesting that some broadening may be due to transient aggregation. The T_2 values and ^{15}N (*39*) NOE values were uniform across the RHCC sequence, indicating that there was little internal motion on the microsecond time scale. At this point, the exact origin of the line broadening was unknown; however, it was clear that NMR resonance assignment and structure determination of RHCC were going to be more challenging than one would normally expect for a dimer of 40 amino acid residues (MW ~ 10000), but a great deal of effort was invested because of the importance of the structure. NMR spectra have been recorded for coiled-coil domains of similar size, suggesting that axial asymmetry was not likely to be an impediment for structure determination (*40*−*42*).

To determine resonance assignments of RHCC, a variety of NMR spectra were collected on unlabeled, ^{15}N-labeled, ^{15}N- and ^{13}C-labeled, and ^{12}C- and ^{13}C-labeled samples. The ^{1}H−^{15}N HSQC spectra of selectively lysine-labeled and selectively leucine-labeled samples were also helpful (*37*). Missing resonances mostly belong to presumably less-ordered residues at the N- and C-termini, although some resonances also could not be observed or resolved for several residues in the C-terminal half. The backbone assignments of N, NH, Cα, and Hα atoms were 90% completed (Table 1S of the Supporting Information).

Previous CD analysis clearly showed that RHCC is an α-helical protein (*17*). Consistent with the CD analysis, most of the Hα chemical shifts of the amino acids showed an upfield shift with respect to the random coil values (Figure 3A), the Cα chemical shifts showed downfield shifts, and most Cβ shifts showed upfield shifts (Figure 2S of the Supporting Information), which reflect the helical configuration of the protein (*43, 44*). In general, the N-terminal half showed greater secondary shifts than the C-terminal half, suggesting stronger helix formation.

Backbone torsion angles of RHCC were predicted by TALOS (*45*) on the basis of matching the Cα, Cβ, N, and Hα chemical shifts of three consecutive residues to patterns observed in a database of proteins of known structure (*45*). NOE distance constraints and local dihedral angle measurements from TALOS were insufficient to derive satisfactory structures. Residual dipolar coupling (RDC) information proved to be very useful for deriving structures with acceptable precision.

The N-terminal (residue S450) and C-terminal (residues L484−M489) regions were poorly defined as few restraints per residue were observed. Elsewhere, one-bond RDCs between amide hydrogens and amide nitrogens were similar with a value of approximately −19 Hz, consistent with the structure of a typical helix in which the amide nitrogen forms a hydrogen bond to the carbonyl of residue $i - 4$ such that the orientation of each N−H vector is the same and parallel to the long axis of the helix. Residues at positions *a* and *d* had slightly smaller RDC values (−23 to −24 Hz), consistent with observations made before on other coiled coils where the portion of the helix at the dimer interface is slightly compressed while those facing outside are stretched (*46*).

Structure calculation was initiated on the monomer starting from an extended chain conformation using CNS (*29*). A subset of 323 distance restraints was used for calculations that were then refined using RDC data (*47*). If the N- and C-terminal regions are excluded, the root-mean-square deviations of the 30 structures against their mean coordinates were 0.43 Å for backbone atoms and 1.16 Å for heavy atoms. Most ϕ and ψ backbone torsion angles were within the allowed region of the Ramachandran plot (Table 1). The structure of RHCC reveals a slightly curved α-helix from residue T452 to N483. The C-terminal region from L484 to M489 was not well-defined, as expected given the limited number of NOE restraints per residue. One possible explanation is that this region is not well-structured, thus giving many fewer NOEs, which agrees with several unobservable resonances in this region and, for the resonances that could be seen, the approach to zero secondary chemical shifts. Because a limited proteolysis study using trypsin indicates that R487 is protected, suggesting that it lies in the structured core (*17*), the structure N-terminal to this residue (probably N-terminal to N483) may block access by trypsin. The C-terminal region from L484 to M489 is important, however, for coiled-coil stability, as a peptide containing residues S450−N483 lacked dispersion in its ^{1}H NMR spectrum and

Table 1: NMR Structural Data and Refinement Statistics

	RH monomer	RH dimer
no. of experimental restraints		
no. of distance restraints from NOEs	323	1081
no. of dihedral angle restraints	78	153
no. of RDCs	30	68
total no. of experimental restraints	431	1302
rms deviations from experimental data		
average distance restraint violation (Å)	0.008 ± 0.002	0.007 ± 0.001
distance restraint violations of >0.5 Å	0.0 ± 0.0	0.0 ± 0.0
average dihedral angle restraint violation	0.40 ± 0.11	0.68 ± 0.19
dihedral angle restraint violations of >5°	0.0 ± 0.0	0.0 ± 0.0
rms deviations from ideal stereochemistry		
bonds (Å)	0.0032 ± 0.0001	0.0034 ± 0.0001
angles (deg)	0.41 ± 0.03	0.48 ± 0.05
impropers (deg)	0.37 ± 0.06	0.54 ± 0.07
Ramachandran analysis of the structures		
residues in favored regions	90.9%	83.6%
residues in additionally allowed regions	9.1%	16.3%
residues in generously allowed regions	0.0%	0.1%
residues in disallowed regions	0.0%	0.0%
Lennard-Jones potential energies		
overall (kcal/mol)	−96 ± 18	−116 ± 52
coordinate precision (Å)[a]		
backbone	0.43 ± 0.11	0.59 ± 0.13
all heavy atoms	1.16 ± 0.14	1.16 ± 0.16

[a] After superimposition of residues 453−484.

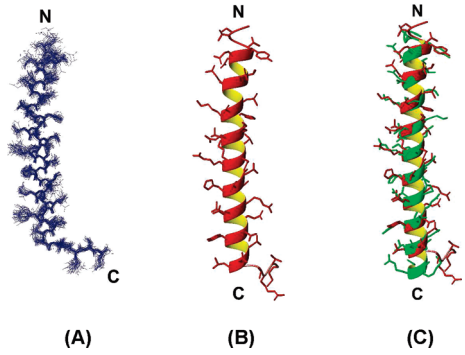

FIGURE 4: Three-dimensional structures of the monomer of RHCC. (A) Bundle of 30 superimposed in stereo (backbone atoms of Y453−L384). (B) Representative structure. (C) Comparison of the monomer with the corresponding residues in the X-ray structure of the Rab11-FIP2−Rab11 complex. The NMR structure is colored red and the X-ray structure green. The backbone rms deviation after superposition of residues C453−L484 was 0.98 Å.

exhibited little CD signal at 222 nm indicative of helix formation (data not shown). Residues L484−M489 exhibited residual dipolar coupling constants that were approximately the same as those of the helical residues closer to the N-terminus. However, their secondary chemical shifts and NOEs typical of helical conformations were weaker, indicating formation of a transient helix. The line widths of peaks in this region were slightly broader than elsewhere in the molecule.

A superposition of the mean structure of the backbone of the monomer to the structure bound to Rab11 had a rms deviation of 0.98 Å (Figure 4B). The differences in side chain conformations are not likely to be significant, because few stereospecific assignments or χ_1 angle determinations were

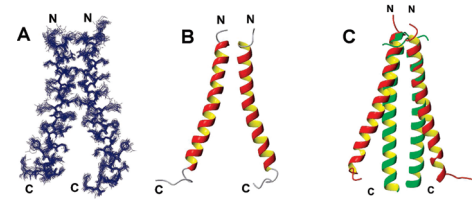

FIGURE 5: Three-dimensional structures of the dimer of RHCC. (A) Bundle of 30 superimposed (backbone atoms of Y453−L484). (B) Representative structure. (C) Comparison of a dimer of RHCC with the corresponding residues in the X-ray structure of the Rab11-FIP2−Rab11 complex. The NMR structure is colored red, whereas the X-ray structure is colored green.

conducted for the NMR structure and thus the side chain conformations were underdetermined. The slightly bent helix body is consistent with the supercoiled dimeric nature of the protein and with the crystal structure.

Only one set of NMR resonances corresponding to RHCC was observed, providing evidence that this dimer is symmetric. The most often violated NOE measurements during the calculation of the monomeric structure were centered on residues Y453, V456, L460, and H463. These NOEs were then reintroduced in the calculation as 18 intermonomer restraints for violations larger than 2 Å and as nine ambiguous restraints (intra- or intermonomer) for violations smaller than 1 Å. These residues were also observed in the X-ray structure to be at the dimer interface. In addition, a few interchain NOEs primarily involving Y453 were obtained from ^{12}C-filtered/^{13}C-selected 3D NOESY spectra designed to measure NOEs between one chain that was unlabeled and the other that was labeled with ^{13}C, although the signal-to-noise ratio in this experiment was too low to be of much use. They were characteristic of side chain packing of the residues in heptad repeats and consistent with the crystal structure. Structures of the dimer were calculated using a total of 1302 restraints, including 1081 NOEs, 153 dihedral restraints, and 68 $^1J_{NH}$ residual dipolar couplings. The final total energy was −116.4 kcal/mol, and the backbone rms deviation of superimposed structures was 0.59 ± 0.13 Å. More than 83% of residues had favored ϕ and ψ torsion angles by PROCHECK analysis, and therefore, the structure was of high quality (Table 1).

A ribbon diagram of a backbone superposition of 30 structures and a representative structure shows the expected coiled-coil structure in the N-terminal half of the molecule, but with fraying of the coiled-coiled structure in the C-terminal half (Figure 5). Analysis of the distance difference matrix of RHCC unbound and bound to Rab11 shows that while the monomeric units have the same structure and the N-terminal halves of the dimers have the same structure the C-terminal halves of the dimers have different structures (Figure 3S). Consistent with the weaker secondary chemical shifts, most of the differences arise from a lack of experimental data specifying the contacts between the helices because of an increased level of motion in the C-terminal half. Consistent with the weaker secondary chemical shifts, most of the differences arise from a lack of experimental data specifying the contacts between the helices because of an increased level of motion in the C-terminal half. Although the deviation in the C-terminal half can partially be explained by poor chemical shift dispersion and fewer NOE distance restraints, some of the differences in the structure (in the

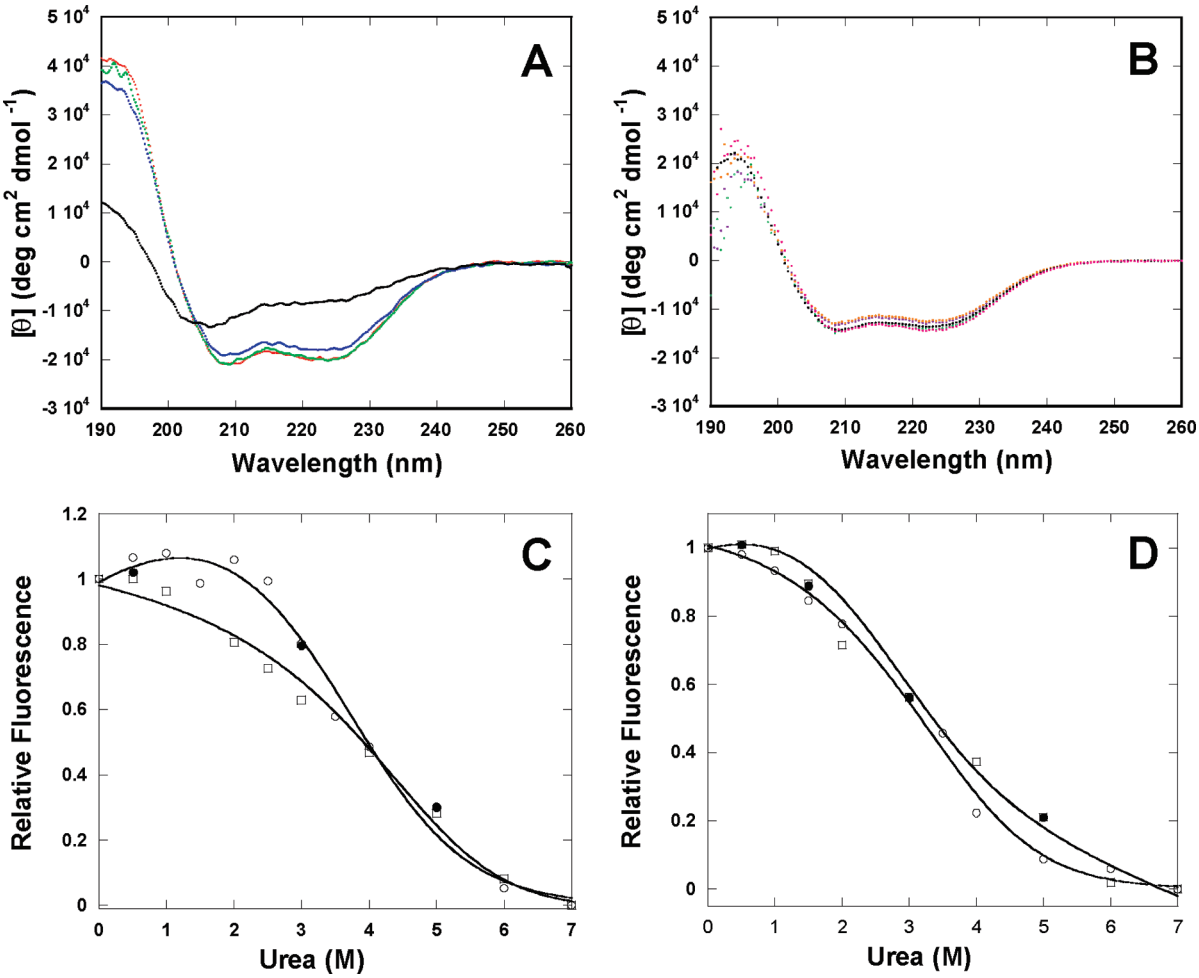

FIGURE 6: Stability of RHCC and its H463A mutant to pH and urea. (A) CD spectra of RHCC at pH 4.0 (black), 6.5 (blue), 7.0 (green), and 8.0 (red). (B) CD spectra of H463A at pH 3.3, 3.9, 6.3, 6.8, and 7.3. (C) Equilibrium unfolding data for RHCC (○) and H463A (□) at pH 7.5. (D) Equilibrium unfolding data of RHCC (○) and H463A (□) at pH 4.0. Corresponding refolding data are shown as filled symbols. Data were measured by recording the fluorescence average emission wavelength as a function of urea concentration. The protein concentrations were 5 μM. Solid lines represent fits to the data using a dimer-to-monomer unfolding model that was used to derive the $\Delta\Delta G_{H_2O}$ values described in the text.

absence of Rab11) and the structure when bound to Rab11 are obvious from analysis of the RDC data (Figure 3B). For example, residues R487 and V488 have experimental RDC values that are near zero, consistent with averaging of the NH vector in solution, while the RDC values calculated from the X-ray structure are approximately −20 Hz, consistent with those residues being in an α-helix. The most striking finding was that the residues that directly contact Rab11 in the crystal structure correspond to those less defined in the NMR structure. For example, Y480 and I481, which are highly conserved residues in RH domains that form an extended hydrophobic surface with Rab11 that is essential to stabilization of the complex in X-ray structure (*9*), exhibit fewer than 10 NOE cross-peaks per residue in NMR data. In addition, the side chain of Y480 makes a hydrogen bond with the backbone of V46 in Rab11. In the complex, the 3_{10}-helix and extended β-sheet of FIP2 align with the β2 strand of Rab11, with residues R487, P493, P499, and Y500 playing a role in stabilizing the conformation of FIP2 in this region (*9*). Thus, the NMR structure of the unbound FIP2 and the X-ray structure of FIP2 while bound to Rab11 are distinctly different.

Assessment of the Role of a Buried Histidine in the RHCC Structure. During optimization of the conditions for NMR analysis, we discovered that pH values below 7 gave NMR spectra of poor dispersion and lower molar ellipticity values in CD spectra (Figure 6A). We attributed the acid destabilization to ionization of H463 found at the hydrophobic *d* position of the heptad repeat of the coiled coil. (The other histidine, H473, is at the *g* position and is exposed to the solvent in both the NMR and X-ray structures.) The pK_a for denaturation was found to be 5.9, consistent with the titration of a histidine residue, although the pK_a was difficult to determine accurately because the intensity of CD spectra could not be reproduced near pH 5.5, the calculated isoelectric point of the peptide. Although a peptide in which H463 was mutated to alanine showed substantially less molar ellipticity, this ellipticity was no longer sensitive to pH (Figure 6B). (Likewise, the intensities of CD spectra at pH values near the calculated pI of this peptide, 5.1, were also variable, mostly likely due to some degree of precipitation.) To examine the pH dependencies in a system that avoids the isoelectric point, equilibrium unfolding in urea was used at pH 7.5 and 4.0 and changes in tertiary structure were monitored by tyrosine fluorescence. The unfolding of the proteins was found to be reversible at both pH values (Figure 6C,D). The data could be fit with a model in which the native dimer unfolds into a monomeric unfolded state

with a single transition (eq 2), and the thermodynamic parameters were obtained from the fits. At pH 7.5, the free energy of unfolding (ΔG_{H_2O}) for RHCC was found to be 12.3 ± 0.1 kcal/mol. The H463A mutant had a ΔG_{H_2O} of 10.6 ± 0.2 kcal/mol, i.e., 1.7 kcal/mol less stable (Figure 6C). At pH 4.0, RHCC (ΔG_{H_2O} of 9.7 ± 0.3 kcal/mol) was less stable than it was at pH 7.5, with a $\Delta\Delta G$ of −2.6 kcal/mol. However, at pH 4, the H463A mutant (ΔG_{H_2O} of 10.7 ± 0.2 kcal/mol) was more stable than wild-type RHCC by 1 kcal/mol (Figure 6D). H463A was equally stable at pH 4.0 and 7.5 (ΔG_{H_2O} values of 10.7 ± 0.2 and 10.6 ± 0.2 kcal/mol, respectively). The data thus demonstrate that H463 is important for acid-induced destabilization.

DISCUSSION

The work presented in this paper is the first to investigate the structure and function of an effector protein, Rab11-FIP2, in the absence of its binding partner Rab11. Although the recently published crystal structure of the effector−Rab11 complex shows a clear picture of interactions after binding, it does not provide information about the structure before binding. Together, these data allow a model in which the binding of FIP family proteins to Rab11 can be described in terms of conformational changes. In the Rab11-FIP2 complex, 10 residues near the C-terminal end of FIP2 form a structure comprising a turn, a 3_{10}-helix, and a β-sheet. However, in the NMR HSQC spectra of the corresponding RH50 construct of unbound FIP2, none of these 10 residues was visible, indicating that they are much less ordered unbound than when in complex with Rab11. Our NMR structure was therefore focused on RHCC, a construct with nine fewer residues at the C-terminus than RH50 (Figure 1A). The results from NMR were consistent with previous results obtained using CD spectroscopy (*17*). Some degree of partial disorder extends further into the coiled coil of RHCC, as some C-terminal residues, while helical, show poor chemical shift dispersion and are not well defined structurally. This partial disorder is consistent with their participation in interacting with Rab11 (Y480, I481, and L485−M489). On the basis of CD data in which an induced α-helical structure was apparent on complex formation, we hypothesized that structure is induced upon Rab11 binding (*17*). Consistent with this hypothesis, these two structures with and without Rab11 in the RHCC covered area suggest that the change does not result from conformational changes within Rab11 (*48*), but from extra helix formation within FIP2 associated with the disorder-to-order transition that is centered on the Rab11 binding domain region of FIP2.

The characterization of dynamics within FIP2 allows several possibilities for regulation of its biological function. One possibility is that levels of unbound protein could be controlled by proteolysis as the less-ordered C-terminal end can be cleaved by trypsin as well as an *Escherichia coli* enzyme with chymotrypsin-like activity (*17*). On the other hand, cellular localization away from cytosolic proteases or binding to other proteins may protect FIP2 in vivo. Another possibility is that the flexibility of FIP2 when unbound allows binding to other proteins, thus altering function. For example, a P85 SH3 binding site is strongly predicted for residues Y500−P502, which would not be accessible when bound to Rab11 (*41*). The dynamics may also allow different choices

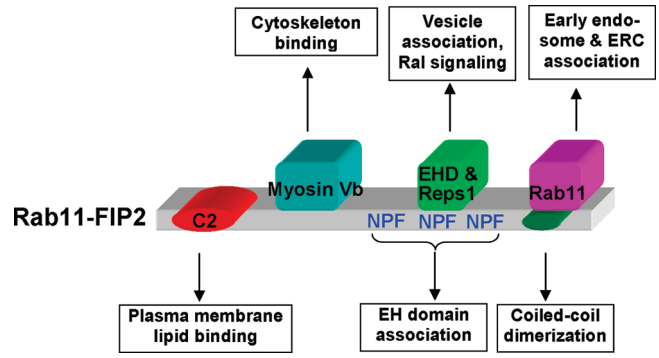

FIGURE 7: Full-length Rab11-FIP2 and its interacting proteins. The domain functions of Rab11-FIP2 are designated underneath the figure, while sites of interactions with various proteins are given above. C2 domains are typically associated with the membranes. Rab11-FIP2's NPF motifs are potential sites for binding EH domain-containing proteins. Two have been identified: EHD1 and close homologues are associated with vesicular structures (*61*), while Reps1 binds RalBP1 as part of the Ral signaling cascade through Ras (*14*). In this paper, we determined the three-dimensional structure of RHCC, which represents the dimeric coiled-coil region. It partially overlaps with the Rab11 binding site. Rab11 is associated with the early endosome and plays a role in vesicle recycling.

to be made more readily than if FIP2 were rigid by allowing the unbound protein to sample a larger conformational space. Such a model would allow one to predict that Rab11 proteins that are on different vesicles or membranes that are separated by various distances could be brought together by FIP2 on formation of a complex with Rab11.

The H463 buried at the RHCC dimer interface impacts the stability of RHCC and may provide an additional mechanism for regulating FIP2 biological function. Buried polar residues in the hydrophobic interface of the coiled-coil proteins are typical as they are important for oligomeric specificity (*49*−*51*), chain orientation, and the kinetics of unfolding (*52*). A neutral histidine 463 at the FIP2 dimer interface, at pH ≥7, preserves the dimeric structure and allows a stable complex with Rab11, which may directly or indirectly mediate vesicle and target membrane fusion (*53*). At lower pH, the protonated histidine destabilizes the dimeric FIP2 and would be predicted to weaken the interaction with Rab11. The histidine-dependent dissociation of dimeric structures has been observed before in other kinds of structures, but we are unaware of ionization of histidines that destabilize formation of a coiled coil (*54, 55*). Several physiological conditions are associated with cellular pH values below pH 7, including hypoxia and apoptosis, although it remains to be determined whether the function of FIP2 in vivo is pH-dependent (*56*−*58*).

The structure of FIP2 and the changes in this structure upon Rab11 binding suggest molecular mechanisms underlying endocytic recycling pathways (Figure 7). The dimeric Rab11-FIP2 appears to act as a scaffold that brings several proteins involved in vesicle sorting in addition to the binding of Rab11 for vesicle recycling (Figure 7). N-Terminal to the coiled coil (residues 453−491) and Rab11 binding domain (residues 477−498) are three NPF sequences (residues 324−326, 406−408, and 440−442) that play a role in recruiting proteins with Eps15 homology domains, such as EHD1 (*59*) and Reps1 (*14*). In the case of Reps1, FIP2 coordinates intracellular trafficking of components of the Ras/Ral signal transduction pathway. The possibility of cross talk

between FIP signaling pathways has been suggested ever since the evidence of the existence of heterodimers of FIPs in cell culture was presented (*11, 60*), yet only homo-oligomers of FIPs are detected in vitro (*60*). The other potential intermolecular binding sites are the myosin Vb binding domain (residues 129−290) that links endosomes to the cytoskeleton and the C2 lipid binding domain (residues 1−129) that links to the plasma membrane and thus regulates cytoskeletal delivery of vesicles to the plasma membrane. Changes in FIP2 structure upon Rab11 binding might change the interactions with other partners such as EHD/Reps1, myosin Vb, and the plasma membrane, subsequently regulating the pathways in which they are involved.

In conclusion, biophysical experiments, a NMR solution structure, and the crystal structure of the complex have together provided a picture of structural and dynamic aspects of the interaction between Rab11 and FIP2. While these studies have improved our understanding of the molecular mechanisms behind Rab11 binding to FIP2, they also suggest that homologues in the FIP family will behave similarly and show disorder-to-order transitions upon binding Rab11.

ACKNOWLEDGMENT

We thank Dr. James Sudmeier for help with setting up 3D NMR experiments.

SUPPORTING INFORMATION AVAILABLE

One table summarizing NMR chemical shift data and three figures of ^{15}N relaxation data, analysis of chemical shifts, and comparison of structures. This material is available free of charge via the Internet at http://pubs.acs.org.

REFERENCES

1. Wang, X., Kumar, R., Navarre, J., Casanova, J. E., and Goldenring, J. R. (2000) Regulation of vesicle trafficking in madin-darby canine kidney cells by Rab11a and Rab25. *J. Biol. Chem. 275*, 29138–29146.
2. Wilcke, M., Johannes, L., Galli, T., Mayau, V., Goud, B., and Salamero, J. (2000) Rab11 regulates the compartmentalization of early endosomes required for efficient transport from early endosomes to the trans-golgi network. *J. Cell Biol. 151*, 1207–1220.
3. Vetter, I. R., and Wittinghofer, A. (2001) The guanine nucleotide-binding switch in three dimensions. *Science 294*, 1299–1304.
4. Ostermeier, C., and Brunger, A. T. (1999) Structural basis of Rab effector specificity: Crystal structure of the small G protein Rab3A complexed with the effector domain of rabphilin-3A. *Cell 96*, 363–374.
5. Zhu, G., Zhai, P., Liu, J., Terzyan, S., Li, G., and Zhang, X. C. (2004) Structural basis of Rab5-Rabaptin5 interaction in endocytosis. *Nat. Struct. Mol. Biol. 11*, 975–983.
6. Shiba, T., Koga, H., Shin, H. W., Kawasaki, M., Kato, R., Nakayama, K., and Wakatsuki, S. (2006) Structural basis for Rab11-dependent membrane recruitment of a family of Rab11-interacting protein 3 (FIP3)/Arfophilin-1. *Proc. Natl. Acad. Sci. U.S.A. 103*, 15416–15421.
7. Wu, M., Wang, T., Loh, E., Hong, W., and Song, H. (2005) Structural basis for recruitment of RILP by small GTPase Rab7. *EMBO J. 24*, 1491–1501.
8. Eathiraj, S., Pan, X., Ritacco, C., and Lambright, D. G. (2005) Structural basis of family-wide Rab GTPase recognition by rabenosyn-5. *Nature 436*, 415–419.
9. Jagoe, W. N., Lindsay, A. J., Read, R. J., McCoy, A. J., McCaffrey, M. W., and Khan, A. R. (2006) Crystal structure of rab11 in complex with rab11 family interacting protein 2. *Structure 14*, 1273–1283.
10. Hales, C. M., Griner, R., Hobdy-Henderson, K. C., Dorn, M. C., Hardy, D., Kumar, R., Navarre, J., Chan, E. K., Lapierre, L. A., and Goldenring, J. R. (2001) Identification and characterization of a family of Rab11-interacting proteins. *J. Biol. Chem. 276*, 39067–39075.
11. Wallace, D. M. (2002) The novel Rab11-FIP/Rip/RCP family of proteins displays extensive homo- and hetero-interacting abilities. *Biochem. Biophys. Res. Commun.,* 909–915.
12. Lindsay, A. J., Hendrick, A. G., Cantalupo, G., Senic-Matuglia, F., Goud, B., Bucci, C., and McCaffrey, M. W. (2002) Rab Coupling Protein (RCP), a novel Rab4 and Rab11 effector protein. *J. Biol. Chem. 277*, 12190–12199.
13. Prekeris, R., Klumperman, J., and Scheller, R. H. (2000) A Rab11/Rip11 protein complex regulates apical membrane trafficking via recycling endosomes. *Mol. Cell 6*, 1437–1448.
14. Cullis, D. N., Philip, B., Baleja, J. D., and Feig, L. A. (2002) Rab11-FIP2, an adaptor protein connecting cellular components involved in internalization and recycling of epidermal growth factor receptors. *J. Biol. Chem. 277*, 49158–49166.
15. Hales, C. M., Vaerman, J.-P., and Goldenring, J. R. (2002) Rab11 Family Interacting Protein 2 associates with Myosin Vb and regulates plasma membrane recycling. *J. Biol. Chem. 277*, 50415–50421.
16. Lindsay, A. J., and McCaffrey, M. W. (2002) Rab11-FIP2 functions in transferrin recycling and associates with endosomal membranes via its COOH-terminal domain. *J. Biol. Chem. 277*, 27193–27199.
17. Wei, J., Fain, S., Harrison, C., Feig, L. A., and Baleja, J. D. (2006) Molecular dissection of Rab11 binding from coiled-coil formation in the Rab11-FIP2 C-terminal domain. *Biochemistry 45*, 6826–6834.
18. Griffey, R. H., Redfield, A. G., Loomis, R. E., and Dahlquist, F. W. (1985) Nuclear magnetic resonance observation and dynamics of specific amide protons in T4 lysozyme. *Biochemistry 24*, 817–822.
19. Alexander, P., Faneshtock, S., Lee, T., Orban, J., and Bryan, P. (1992) Thermodynamic analysis of the folding of streptococcal protein G IgG-binding domains B1 and B2: Why small proteins tend to have high denaturation temperatures. *Biochemistry 31*, 3597–3603.
20. Muhandiram, D. R., and Kay, L. E. (1994) Gradient-enhanced triple-resonance three-dimensional NMR experiments with improved sensitivity. *J. Magn. Reson., Ser. B 103*, 203–216.
21. Clubb, R. T., and Wagner, G. (1992) A triple-resonance pulse scheme for selectively correlating amide ^{1}HN and ^{15}N nuclei with the ^{1}H alpha proton of the preceding residue. *J. Biomol. NMR 2*, 389–394.
22. Grzesiek, S., Dobeli, H., Gentz, R., Garotta, G., Labhardt, A. M., and Bax, A. (1992) ^{1}H, ^{13}C, and ^{15}N NMR backbone assignments and secondary structure of human interferon-γ. *Biochemistry 31*, 8180–8190.
23. Hansen, M. R., Mueller, L., and Pardi, A. (1998) Tunable alignment of macromolecules by filamentous phage yields dipolar coupling interactions. *Nat. Struct. Biol. 5*, 1065–1074.
24. Vuister, G. W., Kim, S.-J., Wu, C., and Bax, A. (1994) 2D and 3D NMR study of phenylalanine residues in proteins by reverse isotopic labeling. *J. Am. Chem. Soc. 116*, 9206–9210.
25. Kay, L. E., Torchia, D. A., and Bax, A. (1989) Backbone Dynamics of Proteins as studied by ^{15}N inverse detected heteronuclear NMR spectroscopy: Application to staphylococcal nuclease. *Biochemistry 28*, 8972–8979.
26. Dayie, K., and Wagner, G. (1995) Relaxation-rate measurements for N-15-H-1 groups with pulse-field gradients and preservation of coherence pathways. *J. Magn. Reson., Ser. A 111*, 121–126.
27. Agou, F., Ye, F., Goffinont, S., Courtois, G., Yamaoka, S., Israel, A., and Veron, M. (2002) NEMO trimerizes through its coiled-coil C-terminal domain. *J. Biol. Chem. 277*, 17464–17475.
28. Al-Hashimi, H. M., Bolon, P. J., and Prestegard, J. H. (2000) Molecular symmetry as an aid to geometry determination in ligand protein complexes. *J. Magn. Reson. 142*, 153–158.
29. Brunger, A. T., Adams, P. D., Clore, G. M., DeLano, W. L., Gros, P., Grosse-Kunstleve, R. W., Jiang, J. S., Kuszewski, J., Nilges, M., Pannu, N. S., Read, R. J., Rice, L. M., Simonson, T., and Warren, G. L. (1998) Crystallography & NMR system: A new software suite for macromolecular structure determination. *Acta Crystallogr. D54*, 905–921.
30. Liu, Y., Liu, Z., Androphy, E., Chen, J., and Baleja, J. D. (2004) Design and characterization of helical peptides that inhibit the E6 protein of papillomavirus. *Biochemistry 43*, 7421–7431.
31. Zweckstetter, M., and Bax, A. (2000) Prediction of sterically induced alignment in a dilute liquid crystalline phase: Aid to protein structure determination by NMR. *J. Am. Chem. Soc. 122*, 3791–3792.

32. Laskowski, R. A., Rullmannn, J. A., MacArthur, M. W., Kaptein, R., and Thornton, J. M. (1996) AQUA and PROCHECK-NMR: Programs for checking the quality of protein structures solved by NMR. *J. Biomol. NMR 8*, 477–486.
33. Koradi, R., Billeter, M., and Wuthrich, K. (1996) MOLMOL: A program for display and analysis of macromolecular structures. *J. Mol. Graphics 14*, 51–55, 29−32.
34. Bose, K., Yoder, N. C., Kumar, K., and Baleja, J. D. (2007) The role of conserved histidines in the structure and stability of human papillomavirus type 16 E2 DNA-binding domain. *Biochemistry 46*, 1402–1411.
35. Royer, C. A., Mann, C. J., and Matthews, C. R. (1993) Resolution of the fluorescence equilibrium unfolding profile of trp aporepressor using single tryptophan mutants. *Protein Sci. 2*, 1844–1852.
36. Santoro, M. M., and Bolen, D. W. (1988) Unfolding free energy changes determined by the linear extrapolation method. 1. Unfolding of phenylmethanesulfonyl α-chymotrypsin using different denaturants. *Biochemistry 27*, 8063–8068.
37. Wei, J. (2006) Ph.D. Thesis, p 185, Tufts University School of Medicine, Boston, MA.
38. MacKay, J. P., Shaw, G. L., and King, G. F. (1996) Backbone dynamics of the c-Jun leucine zipper: ^{15}N NMR relaxation studies. *Biochemistry 35*, 4867–4877.
39. Al-Hashimi, H. M., Pitt, S. W., Majumdar, A., Xu, W., and Patel, D. J. (2003) Mg^{2+}-induced variations in the conformation and dynamics of HIV-1 TAR RNA probed using NMR residual dipolar couplings. *J. Mol. Biol. 329*, 867–873.
40. Greenfield, N. J., Montelione, G. T., Farid, R. S., and Hitchcock-DeGregori, S. E. (1998) The structure of the N-terminus of striated muscle α-tropomyosin in a chimeric peptide: Nuclear magnetic resonance structure and circular dichroism studies. *Biochemistry 37*, 7834–7843.
41. Gordon-Smith, D. J., Carbajo, R. J., Yang, J. C., Videler, H., Runswick, M. J., Walker, J. E., and Neuhaus, D. (2001) Solution structure of a C-terminal coiled-coil domain from bovine IF_1: The inhibitor protein of F_1 ATPase. *J. Mol. Biol. 308*, 325–339.
42. Walters, K. J., Dayie, K. T., Reece, R. J., Ptashne, M., and Wagner, G. (1997) Structure and mobility of the PUT3 dimer. *Nat. Struct. Biol. 4*, 744–750.
43. Wishart, D. S., Sykes, B. D., and Richards, F. M. (1992) The chemical shift index: A fast and simple method for the assignment of protein secondary structure through NMR spectroscopy. *Biochemistry 31*, 1647–1651.
44. Wishart, D. S., Sykes, B. D., and Richards, F. M. (1991) Relationship between nuclear magnetic resonance chemical shift and protein secondary structure. *J. Mol. Biol. 222*, 1423–1431.
45. Cornilescu, G., Delaglio, F., and Bax, A. (1999) Protein backbone angle restraints from searching a database for chemical shift and sequence homology. *J. Biomol. NMR 13*, 289–302.
46. Mesleh, M. F., Veglia, G., DeSilva, T. M., Marassi, F. M., and Opella, S. J. (2002) Dipolar waves as NMR maps of protein structure. *J. Am. Chem. Soc. 124*, 4206–4207.
47. Tjandra, N., Omichinski, J. G., Gronenborn, A. M., Clore, G. M., and Bax, A. (1997) Use of dipolar ^{1}H-^{15}N and ^{1}H-^{13}C couplings in the structure determination of magnetically oriented macromolecules in solution. *Nat. Struct. Biol. 4*, 732–738.
48. Pasqualato, S., Senic-Matuglia, F., Renault, L., Goud, B., Salamero, J., and Cherfils, J. (2004) The structural GDP/GTP cycle of Rab11 reveals a novel interface involved in the dynamics of recycling endosomes. *J. Biol. Chem. 279*, 11480–11488.
49. Hendsch, Z. S., and Tidor, B. (1994) Do salt bridges stabilize proteins? A continuum electrostatic analysis. *Protein Sci. 3*, 211–226.
50. Barlow, D. J., and Thornton, J. M. (1983) Ion-pairs in proteins. *J. Mol. Biol. 168*, 867–885.
51. Rozwarski, D. A., Gronenborn, A. M., Clore, G. M., Bazan, J. F., Bohm, A., Wlodawer, A., Hatada, M., and Karplus, P. A. (1994) Structural comparisons among the short-chain helical cytokines. *Structure 2*, 159–173.
52. Knappenberger, J. A., Smith, J. E., Thorpe, S. H., Zitzewitz, J. A., and Matthews, C. R. (2002) A buried polar residue in the hydrophobic interface of the coiled-coil peptide, GCN4-p1, plays a thermodynamic, not a kinetic role in folding. *J. Mol. Biol. 321*, 1–6.
53. Akey, D. L., Malashkevich, V. N., and Kim, P. S. (2001) Buried polar residues in coiled-coil interfaces. *Biochemistry 40*, 6352–6360.
54. Cabezon, E., Butler, P. J., Runswick, M. J., and Walker, J. E. (2000) Modulation of the oligomerization state of the bovine F1-ATPase inhibitor protein, IF1, by pH. *J. Biol. Chem. 275*, 25460–25464.
55. Barbar, E., Kleinman, B., Imhoff, D., Li, M., Hays, T. S., and Hare, M. (2001) Dimerization and folding of LC8, a highly conserved light chain of cytoplasmic dynein. *Biochemistry 40*, 1596–1605.
56. Shrode, L. D., Tapper, H., and Grinstein, S. (1997) Role of intracellular pH in proliferation, transformation, and apoptosis. *J. Bioenerg. Biomembr. 29*, 393–399.
57. Gottlieb, R. A., Nordberg, J., Skowronski, E., and Babior, B. M. (1996) Apoptosis induced in Jurkat cells by several agents is preceded by intracellular acidification. *Proc. Natl. Acad. Sci. U.S.A. 93*, 654–658.
58. Xiong, Z. G., Chu, X. P., and Simon, R. P. (2006) Ca^{2+}-permeable acid-sensing ion channels and ischemic brain injury. *J. Membr. Biol. 209*, 59–68.
59. Naslavsky, N., Rahajeng, J., Sharma, M., Jovic, M., and Caplan, S. (2006) Interactions between EHD proteins and Rab11-FIP2: A role for EHD3 in early endosomal transport. *Mol. Biol. Cell 17*, 163–177.
60. Junutula, J. R., Schonteich, E., Wilson, G. M., Peden, A. A., Scheller, R. H., and Prekeris, R. (2004) Molecular characterization of Rab11 interactions with members of the family of Rab11-interacting proteins. *J. Biol. Chem. 279*, 33430–33437.
61. George, M., Ying, G., Rainey, M., Solomon, A., Parikh, P., Gao, Q., Band, V., and Band, H. (2007) Shared as well as distinct roles of EHD proteins revealed by biochemical and functional comparisons in mammalian cells and *C. elegans*. *BMC Cell Biol. 8*, 3.

BI8020197